論文 / 著書情報
Article / Book Information

Title	Building Dampers under Long-Duration Earthquakes or Winds
Authors	Kazuhiko Kasai, Daiki Sato
Citation	The 16th International Advanced School on Wind and Structural Engineering (IAS16), 377-395
Pub. date	2018, 10

Building Dampers under Long-Duration Earthquakes or Winds

Kazuhiko Kasai[a] and Daiki Sato[a]

[a]*Tokyo Institute of Technology, Yokohama City, Japan*

ABSTRACT: In order to study effectiveness of dampers in the super-tall buildings subjected to long-period and long-duration earthquake, four types of full-scale dampers typically used in Japan are examined by the long-duration harmonic loading tests. The test specimens are the so-called oil damper, viscous damper, viscoelastic damper, and steel damper, respectively. Different behavior and variations in their dynamic properties are observed, and they are summarized by referring to distinct materials and mechanisms of the dampers. The viscous and viscoelastic dampers show relatively large variations in the dynamic properties, and simplified evaluation rules to predict the peak cyclic force variations for the dampers are proposed.

KEYWORDS: Response control system, Long-period ground motion, Super-tall building, Cumulative responses, Dynamic Properties, Simplified evaluation rule

1 INTRODUCTION

1.1 *Long-period ground motion and damper*

In recent years, long-period ground motions are considered to occur in large metropolitan cities such as Tokyo, Osaka and Nagoya due to the Nankai Trough [1]. Super-tall buildings with long natural period are prone to sway under long-period ground motion, and duration of shaking tends to be long in the thick plain part of the sedimentary layer. In the 2011 earthquake off the Pacific coast of Tohoku (Tohoku earthquake), it has been reported that super-tall buildings continued to shake for more than 10 minutes due to resonance [2]. Since the Nankai Trough earthquake is presumed to cause super-tall buildings to sway for a long duration with larger ground accelerations, retrofitting measures to existing buildings are urgently proposed.

However, the research on the long period ground motion with long duration, although recognized for long years, is relatively immature. As a result, the majority of existing super-tall buildings are designed to adapt to conventional seismic motion. Long-period ground motions have several times more input energy than design earthquake ground motions, thus, there is a possibility that some buildings will suffer more damage than considered in design. To reduce the response to buildings that are expected to suffer such damage, vibration damping and retrofit with a vibration damper with sufficient energy absorbing capability as a countermeasure against long-period earthquake ground motion would be effective.

Therefore, analytical studies on damping performance of super-tall buildings subjected to long-period ground motion [3-4] and shaking table experiments [5-7] are performed. According to Reference [7], in a super-tall building subjected to long-period seismic motion, majority of energy

concentrates at the beam-column connections subjected to repetitive deformation causing it to be heavily damaged, but these damages can be reduced by dampers.

Dynamic characteristics of the dampers have various dependencies depending on damper type [8], some characteristics may change depending on the input energy and duration, and there is possibility that long-duration repetitive excitations may affect the building response. A great number of researches, for example [9-10], have investigated the dependencies of base-isolation devices under high-amplitude and high-cycle loadings. However, only few studies [e.g., 11], have addressed the vibration dampers, thereby, dependencies are not fully understood.

1.2 *Objective and scope of this study*

As mentioned above, this paper aims to propose a damping design method based on the long-duration harmonic loading tests on four typical full-scale dampers. Based on these results, it is necessary to clarify the change of the dynamic characteristics of the damper. Based on the results of the long-duration harmonic loading experiment conducted with varying amplitude, period, number of cycles, etc., the dynamic characteristics such as the peak damping force, the amount of dissipated energy, equivalent stiffness and viscosity can be determined and can be used for the simple evaluation method [12-13].

Chapter 2 describes the specifications of the four types of damper specimens and the test setup to measure displacement, force, strain, and temperature. Chapter 3 explains the loading conditions and the method of data reduction for the 35 experiments using these dampers. Chapter 4 describes the results of the ideal sinusoidal excitation of the long-duration ground motion for all dampers, amplitude = ±20 mm, period = 4 s, duration = 600 s (150 cycles). In Chapters 5 and 6, based on the experiments with varying amplitudes, cycles, and vibration period, we will discuss the viscous and viscoelastic dampers whose dynamic properties changed greatly as the number of excitation cycles increased, and will propose simplified methods to predict such changes.

2 DAMPER SPECIFICATIONS AND TEST SETUP

In order to verify the characteristics of the four damper types commonly used in Japan (i.e., steel damper, viscous damper, oil damper and viscoelastic damper), the E-Defense full-scale five-story structure shaking table experiments (herein referred as building experiment) were conducted in 2009 [14-17]. To grasp in detail the damper characteristics under ideal boundary conditions, dynamic excitation analyses were performed at Tokyo Institute of Technology using harmonic and non-harmonic wave inputs [18-24]. This paper presents the findings from the long-duration harmonic excitation cases.

The four damper types are explained herein. Dampers used in the building experiment are hereafter referred as D1, D2, and D3 [14-17]. D1 and D2 are located at the exterior frames of the building in the short direction and are of the same damper type. D3 is located at the interior frames of the building in the longitudinal direction and has about twice the capacity of D1 and D2.

2.1 *Oil damper*

The oil damper used in this paper consists of a piston and a cylinder. As the piston reciprocates inside the cylinder, the hydraulic oil begins to flow though the valve in the cylinder, generating flow resistance proportional to the velocity of the piston motion. To avoid bending of the piston, a pin joint is used at the end portion.

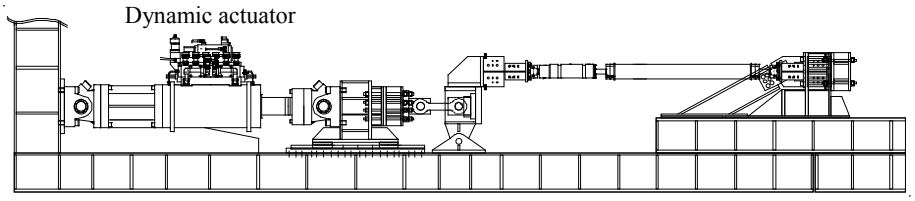

Figure 1. Oil damper setup

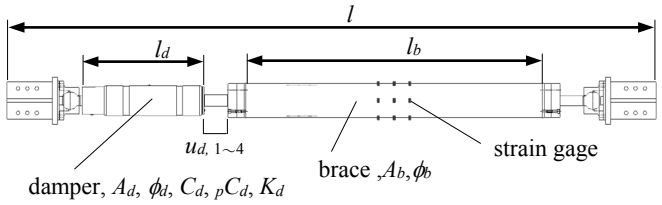

(a) Oil damper side view

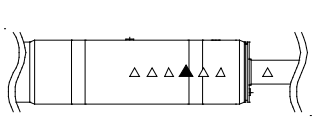

(b) Temperature measurement position

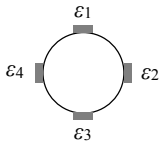

(c) Strain gage position

Figure 2. Oil damper measurement

	story	l (mm)	Damper						Brace			F_{dy} (kN)
			l_d (mm)	A_d (mm^2)	ϕ_d (mm)	C_d Standard value	pC_d Standard value	K_d Standard value	l_b (mm)	A_b (mm^2)	ϕ_b (mm)	
D1 D2	4F	4025	611	2522	140	3.13	0.21	75	2410	3889	140	200
	3F	4025	777	3238	190	6.25	0.42	140	2005	6666	216	400
	2F	3947	777	3238	190	6.25	0.42	140	1813	6666	216	400
	1F	4706	856	4927	274	12.50	0.85	300	2292	10162	267	800
D3	4F	3947	777	3238	190	6.25	0.42	140	1813	6666	216	400
	3F	3947	856	4927	274	12.50	0.85	300	1533	10162	267	800
	2F	3849	856	4927	274	12.50	0.85	300	1399	10162	267	800
	1F	4629	954	8639	310	18.75	1.27	430	2059	16459	319	1200

※ The units of C_d and K_d are kN/(mm/s) and kN/mm, respectively, the standard value of the velocity at F_{dy} is 64 mm/s.

Figures 1 and 2 show the dynamic loading test setup and the measurement locations for oil damper specimen, respectively. Damper deformation u_d is defined in this paper as the stroke measured at the top, bottom, right, left, and right of the cross section of the piston rod exposed. Since the temperature inside the damper cannot be measured directly, the surface temperature is measured by attaching a thermocouple at 7 locations, ± 50 mm, ± 100 mm, + 150 mm with respect to the cylinder center position, and +50 mm from the cylinder end (positive to the left direction). Four strain gages are attached at each of the three cross sections (i = 1 to 3) of the brace, ± 100 mm from the center of the brace. Table 1 indicates the parameters of the oil damper where C_d = internal viscosity, p = secondary viscosity ratio after relief force F_{dy} is reached, and K_d = internal stiffness.

2.2 *Viscous damper*

As the piston reciprocates inside the cylinder of viscous damper, the sealed viscous material (silicone oil) inside flows generating resistance or damping force. This damping force is proportional to the fractional power (α) of velocity. Since $\alpha < 1$, the damper has the property of suppressing the increase of the damping force at high velocity. A pin joint is used at the end portion to avoid bending of the piston.

Figures 3 and 4 show the dynamic loading test setup and the measurement locations for the viscous damper specimen, respectively. Damper deformation u_d is defined in this paper as the stroke measured at the top, bottom, right, left, and right of the cross section of the piston rod exposed. Similar to oil damper, the temperature inside the viscous damper cannot be measured directly, thus, the surface temperature is taken as the temperature of the viscous damper and measured by attaching a thermocouple at 7 locations, ±40 mm, ±80 mm, +100 mm with respect to the cylinder center position and +50 mm from the cylinder end (positive to the left direction). Four strain gages are attached at each of the three cross sections (i = 1 to 3) of the brace at positions of ± 100 mm from the center of the brace. Table 2 indicates the parameters of nonlinear viscosity (see table footnote). The damper forces at velocity 15 cm/s and 30 cm/s are also indicated.

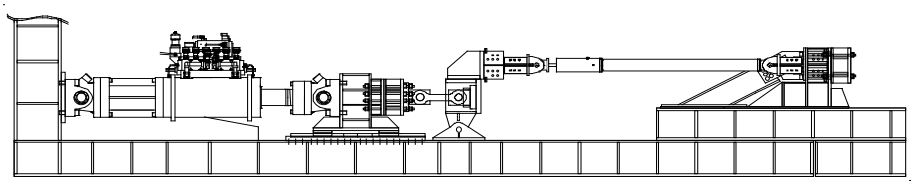

Figure 3. Viscous damper setup

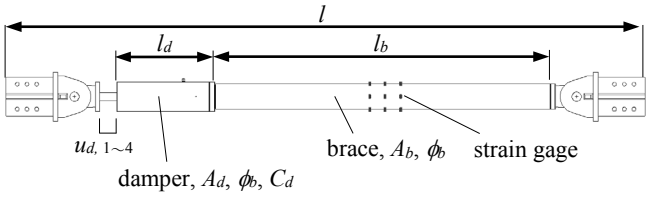

(a) Viscous damper side view

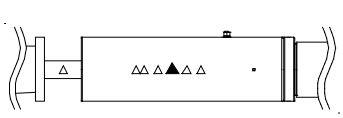

(b) Temperature measurement position

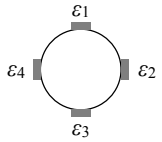

(c) Strain gage position

Figure 4. Viscous damper measurement

Table 2. Parameters of viscous damper

	story	l (mm)	Damper				Brace			$F_{d,max}$ (kN)	
			l_d (mm)	A_d (mm^2)	ϕ_d (mm)	C_d Standard value	l_b (mm)	A_b (mm^2)	ϕ_b (mm)	$\dot{u}_{d,max}$ 15kine	$\dot{u}_{d,max}$ 30kine
D1 D2	4F	4025	535	8034	152	49	2429	9121	140	329	428
	3F	4025	535	8034	152	49	2429	9121	140	329	428
	2F	3947	606	12880	184	98	2104	8320	159	658	856
	1F	4706	606	12880	184	98	2864	8320	159	658	856
D3	4F	3947	606	12880	184	98	2104	8380	159	658	856
	3F	3947	606	12880	184	98	2104	8380	159	658	856
	2F	3849	689	28124	286	196	1542	15323	236	1316	1712
	1F	4629	689	28124	286	196	2322	15323	236	1316	1712

※ The unit of C_d is kN/(mm/s)$^{\alpha}$, the standard value of α is 0.38.

2.3 *Viscoelastic damper*

Viscoelastic dampers (acrylic type) are made by sandwiching viscoelastic materials between laminating steel plates, and energy is absorbed by shear deformation of the viscoelastic materials. Viscoelastic dampers are characterized to have dependencies on temperature and excitation frequency.

Figures 5 and 6 show the dynamic loading test setup and the measurement locations for the viscoelastic damper specimen, respectively. Damper deformation u_d is measured at two locations, i.e., at the top and bottom of the damper cross section. The number of temperature locations for the viscoelastic materials varies with experiment. Thermocouples installed inside the viscoelastic materials can measure the non-uniform distribution of temperature in the thickness direction of the viscoelastic damper. Additionally, six strain gages are installed at the brace. Table 3 indicates the parameters of the viscoelastic damper where d = viscoelastic material thickness, n = number of viscoelastic layers and A_s = total shear area of the laminations.

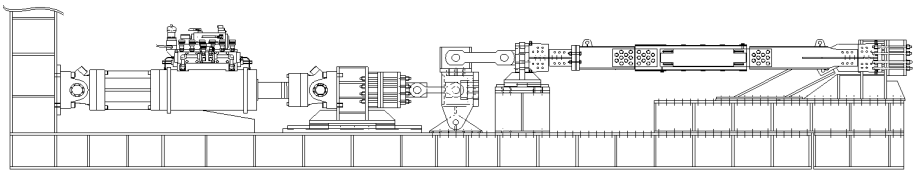

Figure 5. Viscoelastic damper setup

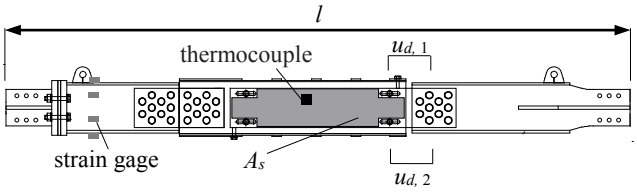

(a) Viscoelastic damper side view

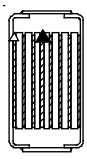

(b) Temperature measurement position

(c) Strain gage position

Figure 6. Viscoelastic damper measurement

	story	l (mm)	As (cm^2)	t (mm)	n	As/t (cm)	Connection member Steel Dimensions (BH)h -b -t_w-t_f	F_{dy} (kN)
D1 D2	4F	4024.5	9120	8	6	11400	BH322-160-19-16	799
	3F	4024.5	9120	8	6	11400	BH322-160-19-16	799
	2F	3946.6	13120	8	8	16400	BH322-160-19-16	1149
	1F	4706.1	13120	9	8	14578	BH322-160-22-16	1212
D3	4F	3946.6	18112	8	8	22640	BH322-150-19-16	1587
	3F	3946.6	18112	8	8	22640	BH322-150-22-16	1587
	2F	3848.9	26000	8	10	32500	BH322-125-32-16	2278
	1F	4628.7	26000	9	10	28889	BH322-150-32-16	2401

2.4 *Steel damper*

The steel damper used is a buckling-restrained brace where buckling of the axially-loaded steel plate is prevented by mortar and encasing rectangular steel pipe. A filler (butyl rubber) is placed between the steel plate and the mortar.

Figures 7 and 8 show the dynamic loading test setup and the measurement locations for the steel damper specimen, respectively. Damper deformation u_d is measured at 4 locations, i.e., each at the top and bottom of the cross sections of the exposed steel brace exposed near loaded and supported ends. Although the thermocouple was not used for the damper in the building experiment, a temperature measurement was conducted by testing the same damper of the same steel material into which thermocouples are inserted (will be called as "posterior analysis damper"). Temperature is measured at three points in total, 700 mm from the center and both ends of the inelastic portion of the brace, where the thermocouple is located between the mortar and the filler. Eight (8) strain gages are installed to the loaded end of the axially-loaded steel plate. Table 4 indicates the parameters of steel damper where l_d = length of the elastic portion, l_e = length of the plastic portion, b_d = width of the elastic portion, b_e = width of the plastic portion, and t_d = thickness of the elastic portion.

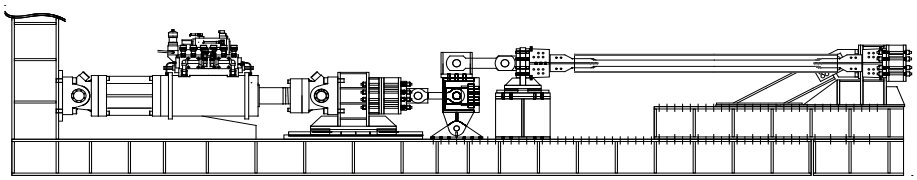

Figure 7. Steel damper setup

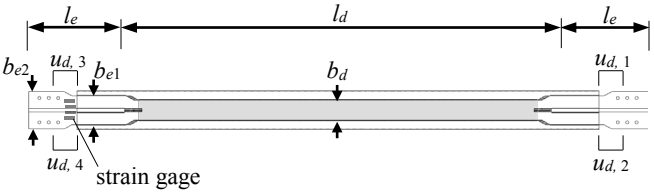

(a) Steel damper side view

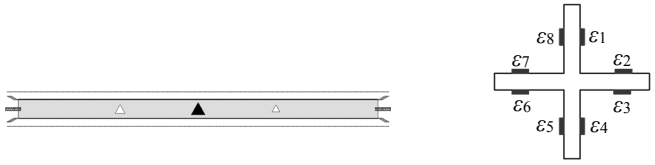

(b) Temperature measurement position (c) Strain gage position

Figure 8. Steel damper measurement

Table 4. Parameters of steel damper

	story	l_d (mm)	l_e (mm)	b_d (mm)	b_e (mm)	t_d (mm)	σ_y (MPa)	$\hat{F}_{dy}$ (kN)	$\hat{u}_{dy}$ (mm)
D1 D2	4F	2900	562.3	88	128/235	16	217	306	3.05
	3F	2900	562.3	88	128/235	16	217	306	3.05
	2F	2750	598.3	116	165/235	19	227	500	3.03
	1F	3600	553.1	116	165/235	19	227	500	3.97
D3	4F	2600	673.3	127	183/235	22	220	615	2.78
	3F	2600	673.3	127	183/235	22	220	615	2.78
	2F	2450	699.5	200	290	22	220	968	2.62
	1F	3300	664.4	200	290	22	217	968	3.52
For post analysis	-	2900	562.3	88	128/235	16	217	306	3.05

3 LOADING CONDITIONS AND DATA REDUCTION METHODS

3.1 *Loading conditions*

Table 5 indicates the damper loading conditions for a total of 35 long-duration harmonic excitations tests. Velocity-dependent dampers such as oil damper, viscous damper and viscoelastic damper can be repeatedly tested without material fatigue damage, thus, the same damper specimen was used for multiple experiments. For the steel damper, loading conditions are limited because the damper manifests small material fatigue in the analysis of the building experiment.

Table 5. Harmonic loading conditions

Damper	Experiment number	Period T (s)	Amplitude u (mm)	Duration t_0 (s)	Number of cycles	Initial temperature θ_0 (℃)	Specimen	References
Oil (O)	O-1	4.0	20	600	150	10	D2-3F	[19]
	O-2	4.0	20	1800	450	14		
	O-3	4.0	20	3600	900	10		
	O-4	4.0	20	4400	1100	13		
	O-5	2.0	20	230	115	15	D3-3F	[21]
	O-6	4.0	10	1200	300	15		
	O-7	4.0	20	600	150	15		
	O-8	4.0	30	400	100	15		
	O-9	6.0	20	900	150	15		
Viscosity (V)	V-1	4.0	20	600	150	10	D1-2F	[20]
	V-2	4.0	20	1800	450	15		
	V-3	4.0	20	3600	900	15		
	V-4	4.0	20	10800	2700	13		
	V-5	2.0	20	230	115	15	D2-2F	[21]
	V-6	4.0	10	1200	300	15		
	V-7	4.0	20	600	150	15		
	V-8	4.0	30	400	100	15		
	V-9	6.0	20	900	150	15		
	V-10	4.0	20	1800	450	26	D3-2F	-
Viscoelasticity (E)	E-1	4.0	20	450	112	21	D3-1F	[18]
	E-2	2.0	16	300	150	22	D1-2F	[22]
	E-3	4.0	8	1200	300	22		
	E-4	4.0	16	600	150	22		
	E-5	4.0	24	400	100	22		
	E-6	6.0	16	900	150	22		
	E-7	2.0	16	300	150	22	D3-3F	
	E-8	4.0	8	1200	300	22		
	E-9	4.0	16	600	150	22		
	E-10	4.0	24	280	70	22		
	E-11	6.0	16	900	150	22		
	E-12	4.0	16	600	150	22	D3-2F	
	E-13	2.86	24.96	66	23	22	D2-3F	[24]
Steel (S)	S-1	4.0	20	924	231	-	D2-2F	[23]
	S-2	4.0	20	1116	279	14	For posterior analysis	

For each of the loading condition, it is assumed that the story drift angle 1/170 rad occurs in a 40-story super-tall building, and the excitation is based the damper deformation u_d = 20 mm and the period T = 4 s [8]. The period of the three velocity-dependent damper types is approximately 2 s to 6 s, and the frequency-dependent steel damper has 4 s. The amplitude is limited to about 10 mm to 30 mm for three velocity-dependent dampers, and 20 mm for steel dampers. In addition, at

period of 4 s, the loading durations of the tests vary from 400 to 4,400 s, 400 to 10,800 s, 280 to 1,200 s and about 1,000 s for the oil damper, viscous damper, viscoelastic damper and steel damper, respectively. For the same order of damper cited above, initial temperature ranges from 10 to 15ºC, 10 to 26ºC, 21 to 22ºC, and 14ºC, respectively, depending on the ambient temperature during the tests. For temperature-dependent viscoelastic damper, we plan further study at low temperature.

At the end of test duration, the damper is rested till its temperature returns to the initial temperature, and checked for damage afterwards by basic loading tests. When no damage is found, the same damper is tested for another loading case. Since the durations of the cases O-3, O-4, V-3, and V-4 exceed the data recording capacity of measuring instruments, loading is delimited every 30 minutes with the short pause for downloading the data.

3.2 *Calculation of damper dynamic properties*

The deformations u_d of the oil dampers, viscosity dampers and viscoelastic dampers are calculated using Equation (1a) and the deformation u_d of steel damper is calculated using Equation (1b). Damping force F_d is calculated using Equation (2).

$$u_d = \frac{\sum_{j=1}^{N_u} u_{d,j}}{N_u}, \quad u_d = \frac{u_{d,1}+u_{d,2}}{2} + \frac{u_{d,3}+u_{d,4}}{2} \tag{1a, b}$$

$$F_d = \frac{\sum_{j=1}^{N_s} \varepsilon_j}{N_s} EA \tag{2}$$

where N_u = number of damper stroke, N_s = number of strain gages placed in one cross section, ε_j = strain at the measurement location, E = Young's modulus (= 206 GPa), and A = cross sectional area at the strain measurement location. The damping forces of the oil damper and viscous damper are calculated from the strain at the center of the brace. In the case of the steel damper, the gages can be attached only at the areas of non-uniform cross section, thus, calibration tests were conducted for each damper and correction coefficient, typically about 1.2, is multiplied to the right side of the Equation (2) [14].

Damper peak force $F_d^{[n]}$ and energy dissipated for each cycle $W_d^{[n]}$ are calculated using Equations (3) and (4). The peak value $F_d^{[n]}$ of cycle n ($\geqq 1$) is calculated from the average of the absolute values of the half wave $2n$ and the half wave $2n+1$, excluding the first half wave immediately after the excitation as shown in Figure 9. The energy dissipated $W_d^{[n]}$ is calculated from the area of the hysteresis loop of each cycle.

$$F_d^{[n]} = \frac{\left| {}_h F_{d,\max}^{\langle 2n \rangle} \right| + \left| {}_h F_{d,\max}^{\langle 2n+1 \rangle} \right|}{2} \tag{3}$$

$$W_d^{[n]} = \sum_{i=1}^{N_D} \frac{\left(F_d^{(i)} + F_d^{(i+1)}\right) \cdot \left(u_d^{(i+1)} - u_d^{(i)}\right)}{2} \tag{4}$$

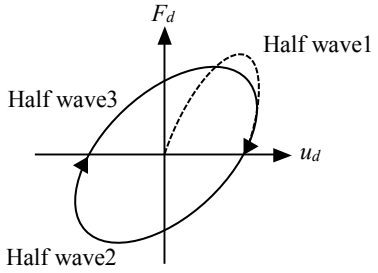

Figure 9. Definition of half wave

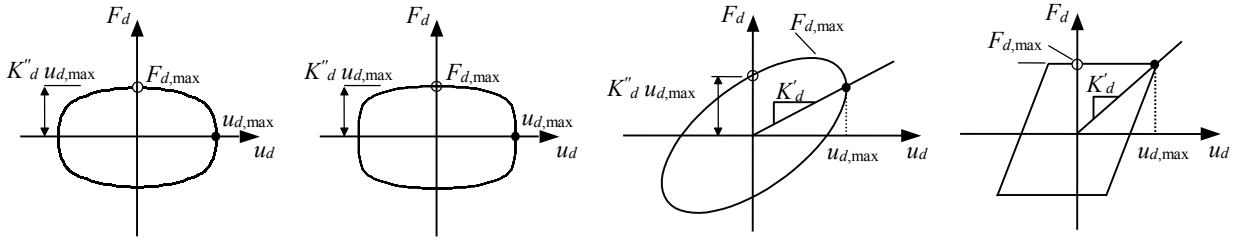

(a) oil (b) viscous (c) viscoelastic (d) steel

Figure 10. Hysteresis in steady state (schematic diagram)

where ${}_hF_{d,max}$ = peak damping force of each half-wave and N_D = number of data of one cycle. Note that ( ), < > , and [ ] stand for step, half wave, and cycle, respectively.

Figure 10 shows the typical hysteresis loops at steady-state response of the four damper types. As shown, the storage stiffness K'_d is taken as the ratio between the force at maximum deformation and the maximum deformation $u_{d,max}$, and the loss stiffness K''_d is taken as the force at $u_d = 0$ divided by $u_{d,max}$ [8]. In this paper, the damper force, energy absorption, storage stiffness, and loss stiffness are referred to as dynamic properties of the damper, and their variations due to long-duration harmonic excitations are examined.

4 LONG-DURATION HARMONIC LOADING TESTS OF FOUR DAMPER TYPES

The decreasing trends of dynamic properties of four damper types under long-duration harmonic loading are presented in this chapter. Discussed here are experiments O-1, V-1, E-1 and S-2 (Table 5) with loading conditions as follows: harmonic excitation period of 4 s, deformation amplitude of ±20mm, and loading duration of 600 s (150 cycles). In the E-1 experiment, the actuator stopped accidentally at 450 s.

Figure 11 shows the hysteresis loops of the four damper types. For the oil damper in Figure 11a, the damper force does not decrease appreciably and the force is stable. For the steel damper in Figure 11d, although the decrease of the damping force is very small after each loading cycle, noticeable decrease can be seen after repetitive loading cycles (i.e., long-duration excitation). The lowering of the damping force in steel damper is attributed to the softening of the filler as the temperature increases [23]. On the other hand, viscous damper in Figure 11c and viscoelastic damper in Figure 11d both show significant decreasing trend of damper force because the viscous and the viscoelastic materials are temperature-dependent and softens with the increase of temperature.

Figure 12 shows the changes of the damper properties with respect to the number of loading cycles. Plotted herein are values at an increment of 10 cycles. The peak damping force $F_d^{[n]}$ is

shown in Figure 12a: The decrease of the oil damper force is very small. That of the steel damper force is relatively large at early loading cycles. That of the viscous damper force gradually decreases over the loading duration. As for the viscoelastic damper, similar behavior to that of steel damper can be seen, wherein large amount of decrease can be seen during the early stage of loading, followed by smaller amount of decrease. For the amount of energy dissipated per cycle $W_d^{[n]}$ as in Figure 12b and loss stiffness $K''_d{}^{[n]}$ as in Figure 12d, the respective dynamic properties of the four damper types decrease in similar manner as that of the peak damping force mentioned above. The storage stiffnesses $K'_d{}^{[n]}$ (Fig. 12c) of the oil damper and viscous damper depend on the hysteresis loop are very small and are disregarded, in contrast to those of the viscoelastic damper and steel damper (Fig. 10).

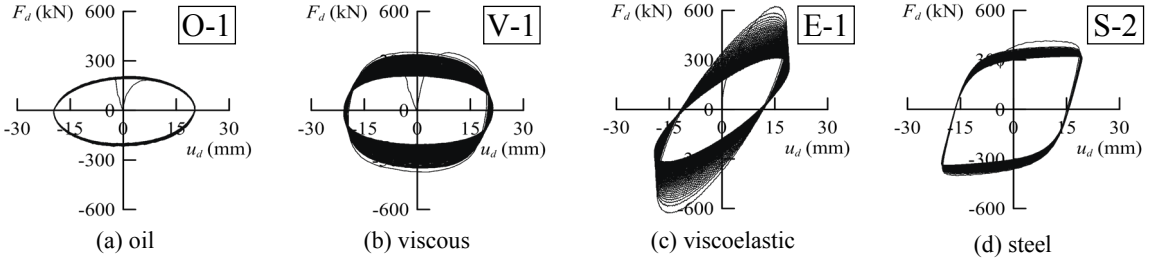

(a) oil (b) viscous (c) viscoelastic (d) steel

Figure 11. Relationship of F_d-u_d (T = 4 s, u_d = 20 mm)

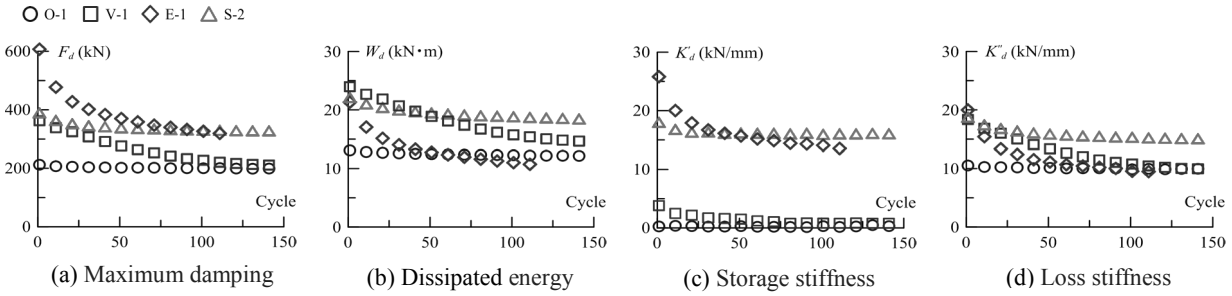

(a) Maximum damping (b) Dissipated energy (c) Storage stiffness (d) Loss stiffness

Figure 12. Dynamic properties vs. number of cycles

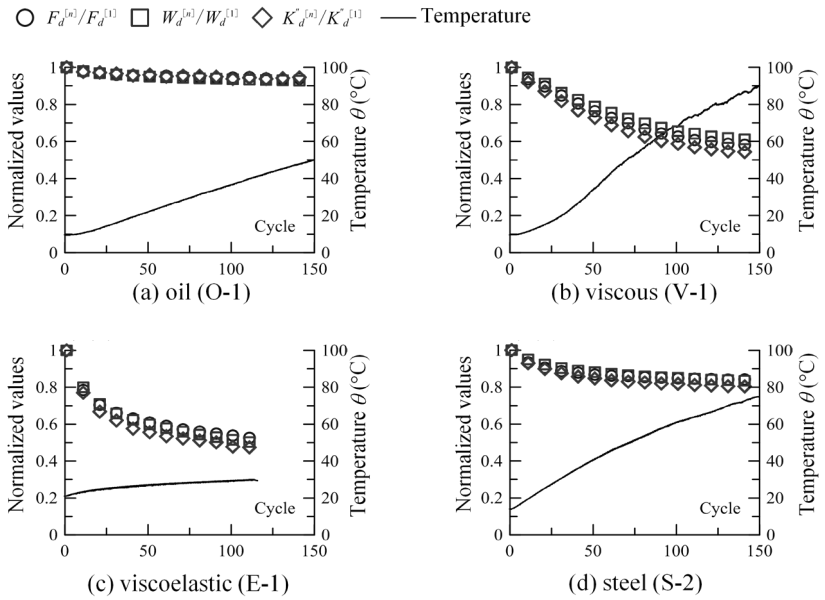

(a) oil (O-1) (b) viscous (V-1)

(c) viscoelastic (E-1) (d) steel (S-2)

Figure 13. Normalized values and temperature vs. number of cycles

To verify the change of dynamic property values with respect to the first cycle, the damping force, the amount of energy dissipated, and the loss stiffness at each cycle are normalized by the value of the first cycle (called as the normalized dynamic property). Figure 13 shows the normalized dynamic properties in relation to the number of cycles. Also shown are the maximum temperatures at the measurement locations (indicated by ▲ in Figs. 2, 4, 6, and 8) in relation to the number of cycles. The decrease of the dynamic properties of oil damper and steel damper are very similar. As for the viscous damper and viscoelastic damper, the decrease rate in loss stiffness per cycle slightly increases which is attributed to slight increase of maximum deformation input as the viscous and viscoelastic materials soften with temperature-rise. However, this variation even with the largest deformation input is very small, 3% for viscous damper and 5% for viscoelastic damper. The amount of temperature increase of viscous damper differs from that of the viscoelastic damper but their dynamic properties decreased similarly after several excitation cycles, i.e., their dynamic properties lower to about 0.5 times of the first cycle after 150 cycles.

Since the decrease rate of each of the dynamic properties except storage stiffness is almost the same, the subsequent chapters focus on the peak damping force and energy dissipation, for the viscous dampers and viscoelastic dampers that exhibited large variations.

5 DYNAMIC PROPERTIES OF VISCOUS DAMPER

This chapter discusses viscous damper tests with sinusoidal loading of different displacement amplitudes and periods. Tests V-1 to V-10 and loading conditions are indicated in Table 5.

Figure 14 shows the hysteresis loops. For the tests V-2 to V-4, the same damper is used. The first cycle hysteresis loops of the three tests are the same, indicating that the viscous damper was not damaged in those tests. The same type of the viscous damper in test V-5 shows larger forces due to relatively large velocity applied (6.3cm/s^2). The large capacity damper in test V-10 shows twice the damper force than that used in V-2. In these tests, the damping forces decreased under the long duration loadings.

Figures 15 shows peak damper forces normalized to that of the first full cycle (n=1, see Sec. 3.2) for all the full cycles applied with (a) peak displacement amplitude 20 mm, and (b) specific period of 4 s, respectively. Initial temperatures for each of the viscous damper are indicated in Table 5. Since the durations for tests V-3 and V-4 are longer than the rest of the tests, only results up to 450 cycles (1800 s) are plotted for comparison. In Figure 15a the normalized peak damping forces are almost the same in the different tests conducted. In Figure 15b for the constant excitation period, the decrease of the peak damper force of the large deformation test V-8 is large at early stage of loading cycles (cf. test V-6). Note also that for large capacity damper in test V-10, the decrease of the damper force is less under the constant excitation period.

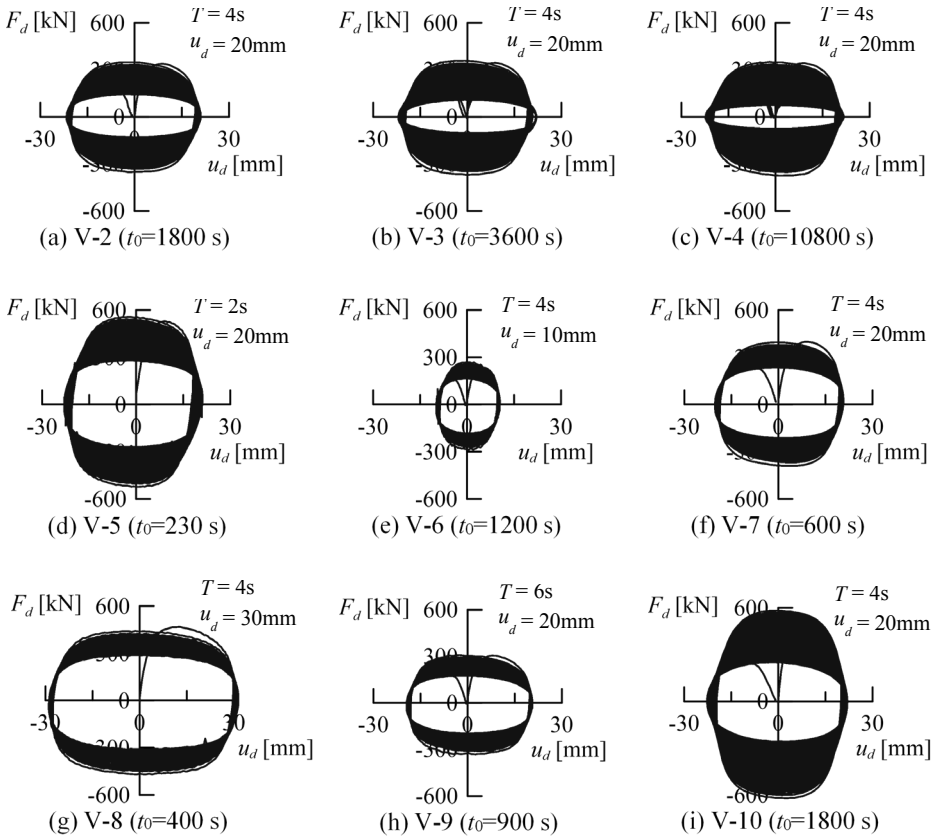

Figure 14. Relationship of F_d-u_d of viscous damper

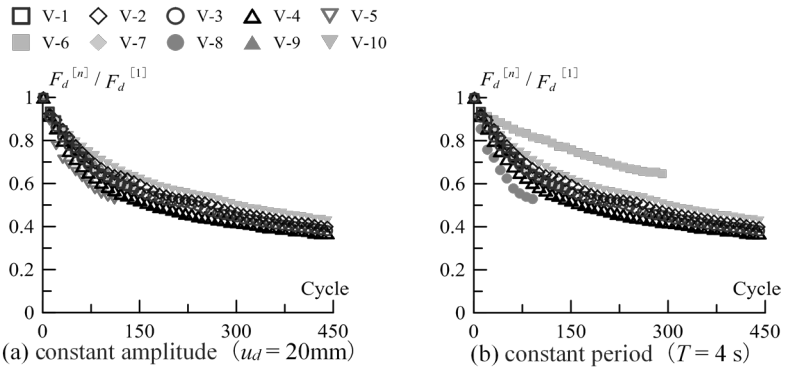

Figure 15. Normalized peak damping force vs. number of cycles

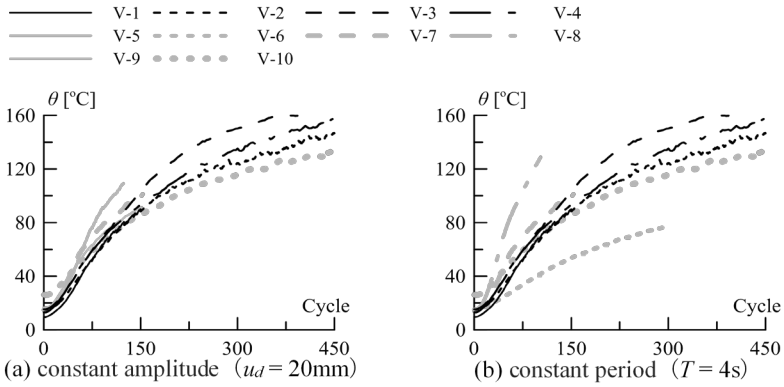

Figure 16. Temperature vs. number of cycles

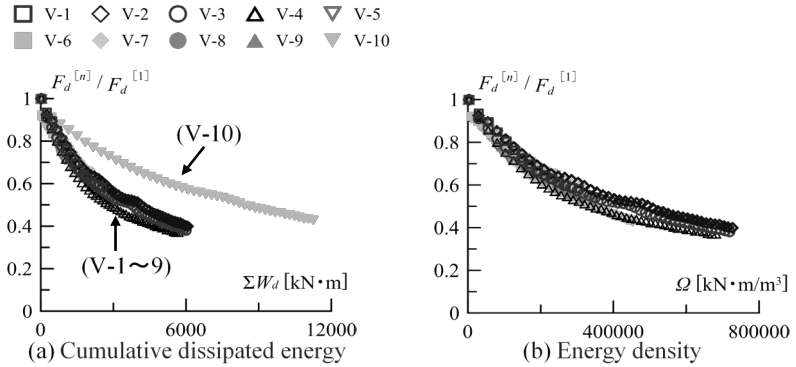

Figure 17. Normalized peak damping force vs. number of cycles

Figure 16 shows the temperature-rise during the tests mentioned above. The generated heat within the viscous damper can be dissipated via the surface of its steel cylinder, and the surface temperature of the steel cylinder rose significantly. For the damper in test V-3, temperature rose to 160ºC after 450 cycles (1800 s) and 200ºC after 900 cycles (3600 s), and it took almost 9 hours before the temperature returned to initial condition. In test V-1, it took 4 hours for its temperature to return to initial condition. In Figure 16a for the peak displacement amplitude 20 mm, temperature-rise is slightly larger in test V-5 applying higher velocity. In Figure 16b for the specific period of 4 s, the temperature in the large deformation test V-8 greatly increased, which is very contrasting to the small deformation test V-6.

By comparing Figures 15 and 16, it is verified that the decrease of peak force is caused by damper temperature-rise. The peak force decreased to nearly 0.4 times that of the first cycle. Based on these, the damper performance due to the long-period ground motion or wind appears to be an important subject to study.

Figure 17a shows the normalized peak damping force vs. dissipated energy ΣW_d of the damper. In tests V-1 to V-9, the dampers of the same capacity are used, and the decrease of the normalized peak damping forces for these dampers are the same regardless of the loading conditions. This is probably because the viscous material absorbs energy, the temperature of the viscous material inside the cylinder rises, and the peak force decreases accordingly. In contrast to tests V-1 to V-9, the trend of decrease is different for the large capacity damper used in test V-10.

These are considered to propose a unified evaluation rule for the viscous dampers with different capacities. The energy density Ω equal to the dissipated energy divided by the volume ${}_{V}V$ of the viscous damper is defined as follows:

$$\Omega = \frac{\sum W_d}{{}_{V}V} \tag{5}$$

where ${}_{V}V$ = volume of the viscous material encased in the viscous damper. The Ω indicates dissipated energy per unit volume of the viscous material and is directly related to the heat generated with the damper [11]. For simplicity, this paper calculates the volume of the viscous material by the length of the damper and the internal cross-sectional area. Figure 17b shows the remarkable correlation between the normalized peak damping forces vs. the energy densityΩ.

Since the temperature-rise of the viscous damper is large, the influence from difference of the initial temperature is believed to be small. Although the tendency may change for the different viscous material and the damper shape, Figure 17b and Equation (5) could predict the deterioration of the damper force under the long-duration loading.

6 DYNAMIC PROPERTIES OF VISCOELASTIC DAMPER

This chapter discusses viscoelastic damper tests with sinusoidal loading of different displacement amplitudes and periods. Tests E-1 to E-13 and loading conditions are indicated in Table 5.

Figure 18 shows the hysteresis loops. In tests E-2 and E-7 with shorter period, the slope of the elliptical hysteresis loop is larger, and it decreases at later cycles. In tests E-3 and E-8 where the peak deformation is small, the force decrease is not very large even for the loading of relatively long duration, which is in contrast to the trends observed from all the other tests.

Figure 19 shows peak damping forces normalized to that of the first full cycle (n=1, see Sec. 3.2) for all the full cycles applied with (a) peak displacement amplitude 16 mm, and (b) specific period of 4 s, respectively. Initial temperatures for each of the viscous damper are indicated in Table 5. In Figure 19a, the normalized peak damping forces decreases abruptly in tests E-2 and E-7 with the short period of excitation, in contrast with tests E-6 and E-11 with the long period.

In Figure 19b for the constant excitation period, the decrease of the peak damping force of the large deformation test E-5 and E-10 is large at early stage of loading cycles (cf. tests E-3 and E-8). It is seen here that the maximum dynamic properties of viscoelastic dampers tend to decrease regardless of the total shear area A_s.

Figure 20 shows significant temperature-rise immediately after the start of the loading. This is because the viscoelastic material is stiffer at the initial condition than its loaded condition, dissipating more energy causing more amount of heat generated during the early stage of loading. Then after about 30 cycles, the temperature increases gradually due to the effect of heat convection where heat is dispersed to the surrounding air through the laminating steel plates. This in turn affects the normalized peak damping force to have gradual decline after about 30 cycles, as seen in Figure 19. In tests E-2 and E-7, the temperature increased up to 35^{o}C.

By comparing Figures 19 and 20, it is verified that the decrease of peak force is caused by the damper temperature-rise. At the maximum temperature, the peak force decreased to 0.4 times that of the first cycle. This is similar to the trend observed for the viscous damper, but it occurs at about one-third number of cycles (cf. Figure 15).

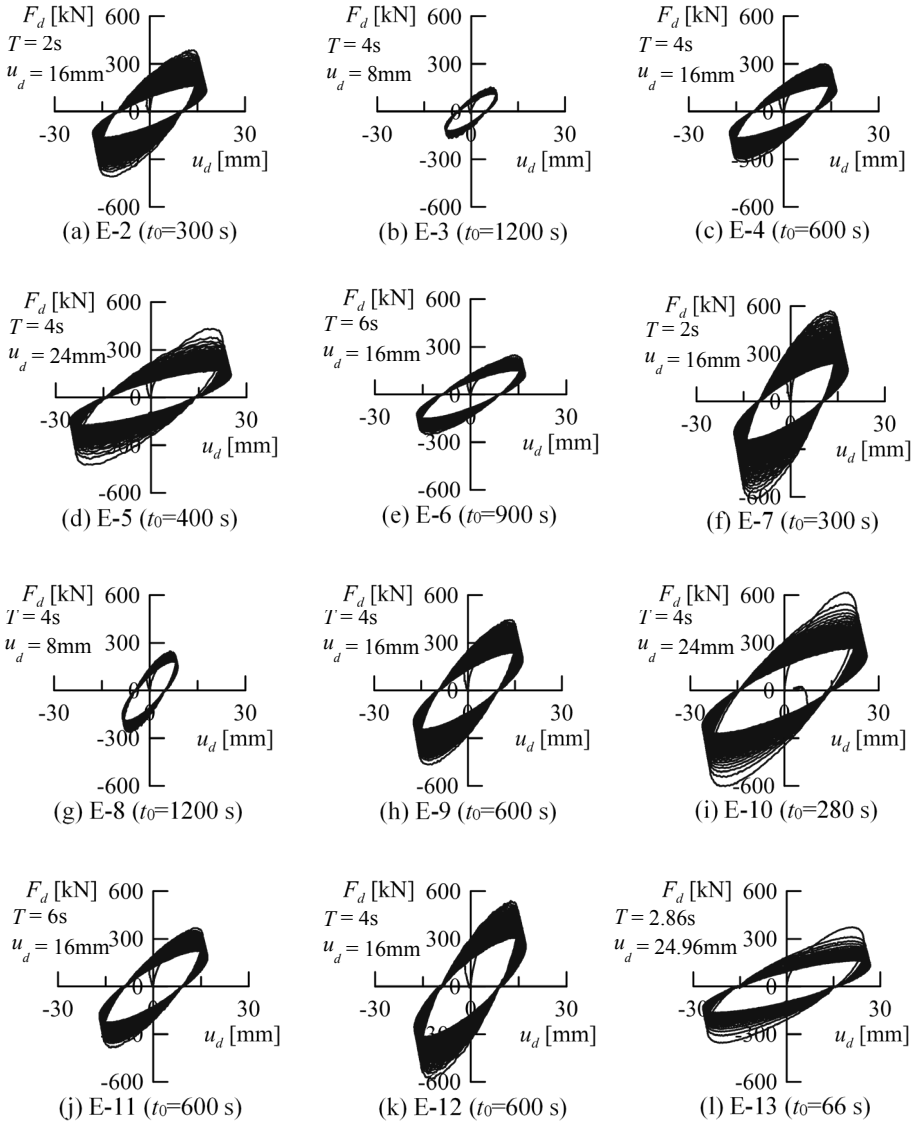

Figure 18. Relationship of F_d-u_d of viscoelastic damper

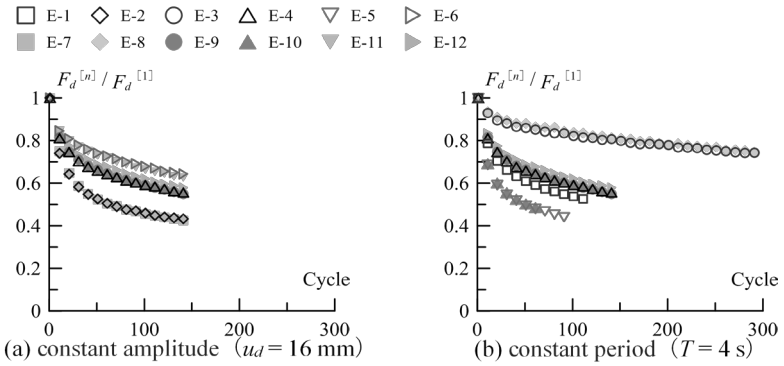

Figure 19. Normalized peak damping force vs. number of cycles

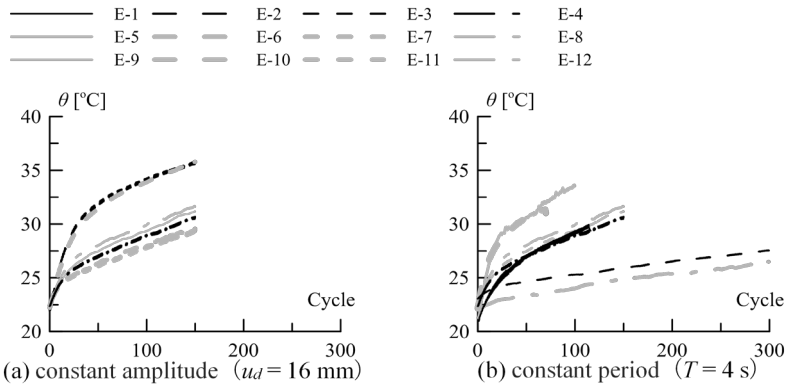

Figure 20. Temperature vs. number of cycles

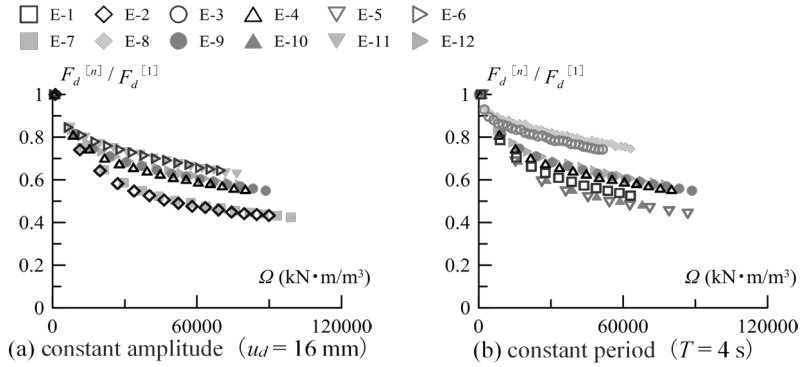

Figure 21. Normalized peak damping force vs. energy density

Figure 21 shows the normalized peak damping force vs. energy density Ω for the volume of the viscoelastic material V. Thus, the correlation is not as strong as observed for the viscous dampers (cf. Figure 17b). Thus, normalized energy density Ω', energy density per unit time and strain, is defined as follows:

$$\Omega' = \frac{\sum W_d}{V} \cdot \frac{\gamma}{T} \tag{6}$$

where γ = peak shear strain and T = excitation period.

Figure 22 shows the remarkable correlation between the normalized peak damping forces vs. Ω', and it is possible to predict the dynamic properties of the viscoelastic dampers regardless of the loading conditions by using Ω'. Note, however, that since the initial temperatures of the viscoelastic dampers are almost equal (21 to 22°C, Section 3.1), effect of the initial temperature will be studied in the future.

The tendency discussed above may change for different viscoelastic materials or damper configurations. However, the normalization proposed can conveniently evaluate deterioration of the damper force capacities during long-duration loading irrespective of various strain amplitudes and periods.

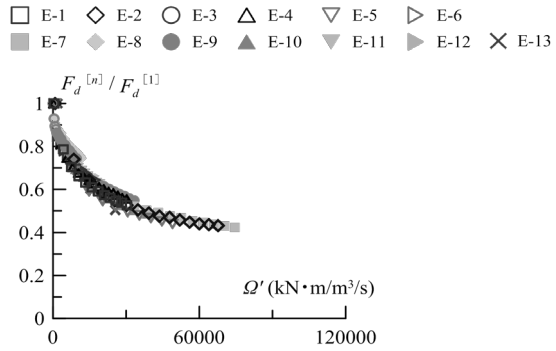

Figure 22. Normalized peak damping force vs. normalized energy density

7 CONCLUSIONS

This study investigated the variations of the dynamic properties of four full-scale dampers types under long-duration harmonic excitations based on the experiments conducted. In addition, a simple evaluation method was proposed to predict the dynamic property of viscous damper and viscoelastic damper under long-duration harmonic loadings. The following are the findings:

(1) From the results of the harmonic excitation tests with period 4 s, deformation amplitude ± 16 to 20 mm, and loading duration of about 600 s, the forces of viscous damper and viscoelastic damper decreased to about 0.5 times those of the first cycle due to the temperature-rise. Oil damper showed small decrease, while steel damper showed large decrease at earlier cycles.
(2) For the viscous dampers, a simple evaluation method using energy density Ω was proposed to predict decrease of the damper force capacities for the various loading conditions and damper capacities.
(3) For the viscoelastic dampers, a simple evaluation method using the modified energy density Ω' was proposed to predict decrease of the damper force capacities for the various loading conditions and damper capacities, by considering the trend different from the viscous damper.

The findings given in this paper are being utilized for the writers' current study on the super-tall building responses under the long-period earthquakes and strong winds.

ACKNOWLEDGMENTS

The authors are grateful to Mr. Sho Nagayama, Mr. Dave M. Osabel, Ms. Xiuyan Liu and Mr. Kazuya Nakamura, graduate students of Sato Laboratory – Tokyo Institute of Technology, for their assistance in the preparation of this paper.

REFERENCES

1 土木学会, 日本建築学会：海溝型巨大地震による長周期地震動と土木・建築構造物の耐震性向上に関する共同提言, 2006.11

2 Architectural Institute of Japan: Protecting High-rises Against Long Period Motions – Wisdom to Share among Designers and Engineers, 2013.11 (in Japanese)
3 Shimada, Y., Sato, D., Nagae, T., Kitamura, H., Fukuyama, K., Kajiwara, K., Inoue, T., Nakashima, M., Saito, T., Fukuwa, N. and Hitaka, T.: Investigation on Partial Install of Hysteretic Dampers into Lower Stories of High-rise Buildings-Retrofitting against Long-period Ground Motion－, Journal of Structural and Construction Engineering (Transactions of AIJ), Vol.75, No.649, pp.549-557, 2010.3 (in Japanese)
4 Kato, T., Sato, D., Sato, T., Kitamura, H., Nagae, T., Ishii, M. and Yoshie, K.: Investigation on Effectiveness and Influence of Lower Partial Retrofitting with Oil Damper or Steel Damper, AIJ Journal of Technology and Design, Vol.21, No.48, pp.533-538, 2015.6 (in Japanese)
5 Nagae, T., Chung, Y., Shimada, Y., Fukuyama, K., Kajiwara, K., Inoue, T., Nakashima, M., Saito, T., Kitamura, H., Fukuwa, N. and Hitaka, T.: Development of Frame Test System to Assess Seismic Performance of High-rise Buildings－E-defense Shaking Table Test－, Journal of Structural and Construction Engineering (Transactions of AIJ), Vol.74, No.640, pp.1163-1171, 2009.6 (in Japanese)
6 Sato, D., Shimada, Y., Ouchi, H., Nagae, T., Kitamura, H., Fukuyama, K., Kajiwara, K., Inoue, T. and Nakashima, M.: Energy Dissipation and Distribution Ratio in a Steel High-rise Building Subjected to Long-period Ground Motions －E-defense Shaking Table Test of Partially Extracted Frame－, Journal of Structural and Construction Engineering (Transactions of AIJ), Vol.75, No.653, pp.1217-1226, 2010.7 (in Japanese)
7 Sato, D., Nagae, T., Ouchi, Y., Shimada, Y., Kitamura, H., Fukuyama, K., Kajiwara, K., Inoue, T., Nakashima, M., Saito, T. and Fukuwa, N.: E-Defense Shaking Table Tests on A Steel High-rise Building Retrofitted by Steel Dampers Against Long-Period Ground Motions, Journal of Structural and Construction Engineering (Transactions of AIJ), Vol.76, No.667, pp.1639-1648, 2011.9 (in Japanese)
8 Japan Society of Seismic Isolation (JSSI): Manual for Design and Construction of Passively-Controlled Buildings, 3rd Edition, 561 pages, 2013.11(in Japanese)
9 Takenaka, Y., Kondo, A., Takaoka, E., Hikita, M., Kitamura, H. and Nakamura, T.: Experimental Study on Heat-mechanics Interaction Behavior of Laminated Rubber Bearings, Journal of Structural and Construction Engineering (Transactions of AIJ), Vol.74, No.646, pp.2245-2253, 2009.12 (in Japanese)
10 Kitamura, H., Hayakawa, S., Takenaka, Y., Takaoka, E. and Murota, N.: Evaluation of the Influence of Heat-mechanics Interaction Behavior in High-damping Rubber Bearings on Seismic Response of Base-isolated Buildings, Journal of Structural and Construction Engineering (Transactions of AIJ), Vol.75, No.655, pp.1365-1644, 2010.9 (in Japanese)
11 Kasai, K., Sato, D., Huang, Y.: Analytical Methods for Viscoelastic Damper Considering Heat Generation, Conduction, and Transfer under Long Duration Cyclic Load, Journal of Structural and Construction Engineering (Transactions of AIJ), No.599, pp.61-69, 2006.1(in Japanese)
12 長山祥, 佐藤大樹, 笠井和彦, 松田和浩：長周期・長時間地震動時における実大ダンパーの特性評価 その1 4種のダンパーの長時間正弦波加振実験による動的特性の推移, 日本建築学会関東支部研究報告集, pp.389-392, 2016.3
13 長山祥, 佐藤大樹, 笠井和彦, 松田和浩：長周期・長時間地震動時における実大ダンパーの特性評価 その2 減衰の違いによる置換正弦波パラメータの傾向および基準化エネルギー密度の提案, 日本建築学会関東支部研究報告集, pp.393-396, 2016.3
14 Kasai, K., Baba, Y., Nishizawa, K., Hikino, T., Ito, H., Ooki, Y. and Motoyui, S.: Test Results for Building with Steel Dampers (3D Shake Table Tests on Full Scale 5-Story Steel Building with Dampers－Part2), Journal of Structural and Construction Engineering (Transactions of AIJ), Vol.77, No.673, pp.499-508, 2012.3 (in Japanese)
15 Kasai, K., Baba, Y., Ito, H., Tokoro, K., Hikino, T., Ooki, Y. and Murai, R.: 3-D Shake Table Tests on Full-scale 5-story Steel Building with Viscoelastic Dampers, Journal of Structural and Construction Engineering (Transactions of AIJ), Vol.77, No.676, pp.985-994, 2012.6 (in Japanese)
16 Kasai, K., Yamagiwa, H., Baba, Y., Ito, H., Hikino, T. and Ooki, Y.: 3-D Shake Table Tests on Full-scale 5-story Steel Building with Oil Dampers, Journal of Structural and Construction Engineering (Transactions of AIJ), Vol.78, No.693, pp.1999-2008, 2013.11 (in Japanese)
17 Kasai, K., Yamagiwa, H., Nishijima, M., Baba, Y., Ito, H., Hikino, T. and Ooki, Y.: 3-D Shake Table Tests on Full-scale 5-story Steel Building with Viscous Dampers, Journal of Structural and Construction Engineering (Transactions of AIJ), Vol.79, No.695, pp.47-56, 2014.1 (in Japanese)
18 後藤尚哉：極大地震を想定した鋼材･粘弾性ダンパーの材料解析モデル構築と制御型ロッキング架構の応答解析, 2012年度東京工業大学修士論文, 2013.3
19 小松祐樹：実大5層建物実験に用いられたオイルダンパーの制振効果および破壊機構に関する研究, 2012年度東京工業大学修士論文, 2013.3
20 Yamamoto, H., Nishijima, M. and Kasai, K.: Limit Performance Test of Viscous Damper (E-Defense Experimental Projects for Steel Buildings－Part 97), Summaries of Technical Papers of Annual Meeting Architectural Institute of Japan, C-1, pp.1343-1344, 2013.8

21 Sugiyama, N., Yamamoto, H. and Kasai, K.: The Loading Experiment of Full-scale Viscous & Oil Damper and Construction of the Analytical Technique (E-Defense Experimental Projects for Steel Buildings－Part 97), Summaries of Technical Papers of Annual Meeting Architectural Institute of Japan, C-1, pp.1015-1016, 2014.9
22 Sato, D., Kasai, K. and Sakaibara, N.: Experiment of Full-scale Viscoelastic Damper and Analysis due to Change in Dynamic Characteristics under Long-Period Ground Motion－Part 104 (E-Defense Experimental Projects for Steel Buildings－Part 104), Summaries of Technical Papers of Annual Meeting Architectural Institute of Japan, C-1, pp.1009-1010, 2014.9
23 Chaya, Y., Kasai, K.: Limit Performance Estimation of Steel Dampers Under Long Period Ground Motion (E-Defense Experimental Projects for Steel Buildings－Part 103), Summaries of Technical Papers of Annual Meeting Architectural Institute of Japan, C-1, pp. 1007-1008, 2014.9
24 長山祥, 佐藤大樹, 笠井和彦, 杉山暢方, 松田和浩：長周期・長時間地震動における実大粘弾性ダンパーの特性評価実験, 日本地震工学会第11回年次大会梗概集, pp.2-10, 2015.11
25 Nakai, A., Nagayama, S., Sato, D., Kasai, K. and Matsuda, K.: Simplified Response Evaluation of Vibration Control Building with Viscous Dampers under Long Period Ground Motion Part1: Outline of Building Model and Damper Location, Summaries of Technical Papers of Annual Meeting Architectural Institute of Japan, B-2, pp.163-164, 2016.8
26 Nagayama, S., Sato, D., Kasai, K. and Matsuda, K.: Simplified Response Evaluation of Vibration Control Building with Viscous Dampers under Long Period Ground Motion Part2: Response Evaluation Considering Change in Dynamic Properties of Viscous Damper, Summaries of Technical Papers of Annual Meeting Architectural Institute of Japan, B-2, pp.165-166, 2016.8